

This is an Open Access document downloaded from ORCA, Cardiff University's institutional repository:<https://orca.cardiff.ac.uk/id/eprint/96471/>

This is the author's version of a work that was submitted to / accepted for publication.

Citation for final published version:

Qin, Yongpeng, Alves, Tiago , Constantine, Jose Antonio and Gamboa, D. 2017. The role of mass wasting in the progressive development of submarine channels (Espirito Santo Basin, SE Brazil). *Journal of Sedimentary Research* 87 (5) , pp. 500-516. 10.2110/jsr.2017.18

Publishers page: <http://dx.doi.org/10.2110/jsr.2017.18>

Please note:

Changes made as a result of publishing processes such as copy-editing, formatting and page numbers may not be reflected in this version. For the definitive version of this publication, please refer to the published source. You are advised to consult the publisher's version if you wish to cite this paper.

This version is being made available in accordance with publisher policies. See <http://orca.cf.ac.uk/policies.html> for usage policies. Copyright and moral rights for publications made available in ORCA are retained by the copyright holders.



THE ROLE OF MASS WASTING IN THE DEVELOPMENT OF SUBMARINE CHANNELS

Research Article

DOI: <http://dx.doi.org/10.2110/jsr.2017.18>

YONGPENG QIN,¹ TIAGO M. ALVES,¹ JOSÉ CONSTANTINE,² AND DAVIDE GAMBOA³

¹ 3D Seismic Lab, School of Earth and Ocean Sciences, Main Building, Cardiff University, Park Place, Cardiff, CF10 3AT, U.K.

² Department of Geosciences, Clark Hall, Williams College, 947 Main Street, Williamstown, Massachusetts 01267, U.S.A.

³ British Geological Survey, Cardiff Office, Columbus House, Village Way, Greenmeadow Springs, Tongwynlais, Cardiff CF15 7NE, U.K.

ABSTRACT: A Pliocene–Quaternary submarine channel system, influenced by localized mass wasting, is investigated using high-resolution 3D seismic data from offshore Espírito Santo Basin, SE Brazil. Three abandoned channels, a channel belt, and a mass-transport deposit (MTD) are recognized in the channel system within a confluence region confined by salt diapirs. In this confluence region, the cross-sectional area (CSA) of the channel system can be up to 1.2 km², i.e., 4 to 10 times larger than other parts of the study area. These significant changes in the architecture and morphology of the channel system resulted from the interaction between mass-wasting processes and turbidity flows. We postulate that a basal erosional scar created by mass-wasting processes was later filled with an MTD. This basal scar was then used as a preferential pathway for turbidity flows, which were captured by its headwall and lateral margins. The interpreted data show that the captured turbidity flows greatly widened the basal scar but caused only small modifications in scar height. This predominance of widening processes over channel incision occurred because part of the MTD in the basal scar was removed downslope by turbidity flows and replaced by channel-fill deposits. This paper shows that important flow-capture processes can predominate in channel confluence regions of continental slopes. Basal scars can capture turbidity flows and facilitate flow channelization, which are key processes for submarine-channel initiation. Importantly, the replacement of MTDs by channel-fill deposits has profound implications for reservoir volumes and net-to-gross ratios in channel systems and partly depends on the properties of the turbidity flows, such as their erosive ability and frequency. The more erosive and frequent flows are captured by the basal scar, the larger is the accommodation space created for subsequent sand-prone turbidites.

INTRODUCTION

Mass-wasting processes have a significant impact on seafloor morphology and sediment distribution on continental slopes (e.g., Hampton et al. 1996; McAdoo et al.

2000; Pickering and Corregidor 2005; Kneller et al. 2016). They evacuate large volumes of sediment and are capable of changing seafloor topography, ultimately controlling the distribution of turbidite sand bodies that form important reservoirs for hydrocarbons (e.g., Pickering and Corregidor 2005; Armitage et al. 2009; Jackson and Johnson 2009; Joanne et al. 2010; Olafiranye et al. 2013; Ortiz-Karpf et al. 2015; Turner 2015; Kneller et al. 2016; Corella et al. 2016).

A variety of sediment accommodation styles associated with mass-transport deposits (MTDs), the common products of mass-wasting processes, have been documented in the literature. For example, the irregular top surfaces of MTDs can create ponded accommodation space for subsequent turbidites (e.g., Moscardelli et al. 2006; Moscardelli and Wood 2008; Alves 2010; Armitage et al. 2009; Jackson and Johnson 2009; Olafiranye et al. 2013). Armitage et al. (2009) further classified three tiers of topographic relief based on the vertical and lateral scales of irregularities on MTD top surfaces: Tier 1 (meters to several meters), Tier 2 (10 m to several tens of meters), and Tier 3 (100 m to several hundreds of meters). Such a topographic hierarchy leads to diverse sediment distribution patterns (Armitage et al. 2009), as variations in the volume of accommodation space on top of MTDs often depend on the internal structure of these latter deposits, particularly on the distribution of megaclasts or blocks, and orientation and scale of faults in their interior (Armitage et al. 2009; Alves 2010; Olafiranye et al. 2013; Ortiz-Karpf et al. 2015; Kneller et al. 2016). Folds and pressure ridges also contribute to the generation of irregularities on the top surfaces of MTDs (Olafiranye et al. 2013; Kneller et al. 2016).

To better understand accommodation space as a function of MTD geometry and internal structure, the interactions between MTDs and turbidity currents have been documented in a number of studies based on outcrop analogues (e.g., Shultz et al. 2005; Lucente and Pini 2008; Jackson and Johnson 2009), seismic data (e.g., Kertznus 2009; Bernhardt et al. 2012; Masalimova et al. 2015; Ortiz-Karpf et al. 2015; Kneller et al. 2016), bathymetric data (Corella et al. 2016), well and core data (Eggenhuisen et al. 2010; Corella et al. 2016), and numerical models (Stright et al. 2013). These studies have shown that turbidity flows can deposit upstream and above MTDs (e.g., Bernhardt et al. 2012; Ortiz-Karpf et al. 2015; Corella et al. 2016) or, instead, can be erosive to create large-scale scours (e.g., Shultz et al. 2005). Furthermore, turbidity flows can be diverted by topographic highs created by MTDs, leading to the generation of new sediment routes (Hansen et al. 2013; Masalimova et al. 2015; Kertznus 2009; Corella et al. 2016). Large-scale mass-wasting events can, therefore, modify the geometry of sedimentary basins and result in rapid shifts in the location of slope depocenters (Lucente and Pini 2008). Kneller et al. (2016) further pointed out that the deflection (and reflection) of turbidity flows, and associated erosion, bypass, and deposition processes, are controlled by: a) the scale and geometry of MTD-associated topographic relief and b) turbidity-flow properties, e.g., thickness, grain-size distribution, and variations in the vertical density of flows (Kneller et al. 2016; Kneller and McCaffrey 1999).

Previous studies focused mainly on the location and pathways of channels influenced by MTDs (e.g., Kertznus 2009; Hansen et al. 2013; Masalimova et al. 2015; Kneller et al. 2016; Corella et al. 2016), but less attention has been paid to the initiation and

development of submarine channels affected by MTD-related topography. The presence of MTDs at the bases of channel systems has been documented on both seismic (e.g., Deptuck et al. 2003; Mayall et al. 2006) and outcrop data (e.g., Macauley and Hubbard 2013; Bain and Hubbard 2016), leading some authors to suggest that seafloor roughness produced by mass-wasting processes can capture and accelerate turbidity flows, facilitating the formation of channels (e.g., Deptuck et al. 2003; Gee et al. 2007; Abdurrokhim and Ito 2013). In fact, flow-capture processes associated with mass wasting have recently been documented in the Gulf of Mexico and the Nile Delta (e.g., Kertznus 2009; Kneller et al. 2016). However, the role of mass-wasting processes in channel initiation and development is still poorly understood due to the lack of good-quality seismic and stratigraphic data. Compared to outcrop studies, which are not ideal for conducting morphological analyses due to their limited exposure, 3D seismic data provide detailed images of MTDs and associated channel-fill deposits (e.g., Bernhardt et al. 2012; Masalimova et al. 2015; Ortiz-Karpf et al. 2015; Kneller et al. 2016).

This study develops a 3D seismic analysis of a Pliocene–Quaternary Rio Doce Channel System, located in the Espírito Santo Basin, SE Brazil (Fig. 1). It presents a case study of turbidity-flow capture processes in a different slope setting compared to previous studies, i.e., in a mid-slope area rather than on the shelf edge (e.g., Kertznus 2009; Kneller et al. 2016). It starts with a summary of geological setting and methodology, followed by a detailed description of the morphology and distribution of an MTD in the study area, and adjacent channel deposition. Finally, we discuss (a) how MTD-related topography affects flow capture and channel initiation and (b) the observed interactions between MTD and turbidity flows, and their implications for reservoir distribution on continental slopes.

GEOLOGICAL SETTING

Tectono-Sedimentary Evolution of the Espírito Santo Basin

The Espírito Santo Basin, located on the SE Brazil continental margin, is bounded by the Abrolhos Bank to the north and the Campos Basin to the south (Fig. 1A). Four tectono-sedimentary stages have been interpreted in the basin: pre-rift, syn-rift, transition, and drift (Ojeda 1982). The pre-rift stage developed from the Late Jurassic to the Early Cretaceous, and is characterized by the deposition of fluvial–lacustrine sediments in depocenters dominated by fault-related subsidence (Ojeda 1982; Chang et al. 1992). During the syn-rift stage (late Berriasian to early Aptian), the Espírito Santo Basin was affected by intense tectonic subsidence and magmatic activity. Following syn-rift tectonics, thick evaporite sequences and marine carbonates predominated during a mid Aptian to Early Albian transitional stage (Ojeda 1982).

The drift stage lasted from the early Albian to the present day in an open marine environment (Ojeda 1982; Chang et al. 1992). Two megasequences were deposited during the drift stage (Mohriak 2003; Fiduk et al. 2004). An early-drift transgressive megasequence records a phase of gradual deepening of the Espírito Santo Basin from the Albian to the end of the Cretaceous. In detail, this megasequence is composed of Albian

shallow-water carbonates and overlying upper Albian to Paleocene muddy and sandy turbidites (Davison 1999; Fiduk et al. 2004; Alves et al. 2009). A late-drift regressive megasequence was deposited from the Eocene to the present day. It is associated with the uplift of coastal mountains, reactivation of rift structures, and episodic magmatic activity, including the emplacement of the volcanic Abrolhos Bank to the north of the study area (Cordani 1970; Demercian et al. 1993; Cobbold et al. 2001; Mohriak 2005; Mohriak et al. 2008). This megasequence is characterized by the deposition of recurrent MTDs (Omosanya and Alves 2013; Gamboa et al. 2010), together with turbiditic channels and lobes, which were sourced from the Abrolhos Bank and inland rivers (Bruhn and Walker 1997; Davison 1999; Alves et al. 2009; Gamboa and Alves 2015).

Salt Tectonics in the Espírito Santo Basin

Salt tectonics exerts a key control on the structure and stratigraphic architecture of the Espírito Santo Basin (Fiduk et al. 2004). Salt movements are associated with thin-skinned extension due to the gravitational gliding of post-salt strata over Aptian evaporites (Demercian et al. 1993), and reveal different styles across the basin (Fiduk et al. 2004). Salt deformation in the proximal domain of the Espírito Santo continental slope is characterized by the development of salt rollers and rafts due to extension (Fig. 2; Demercian et al. 1993; Fiduk et al. 2004; Alves 2012). The transitional mid-slope domain is dominated by salt diapirs (Fig. 2; Fiduk et al. 2004). Basinward, allochthonous salt canopies and overhangs predominate due to local compressional stresses (Fig. 2; Fiduk et al. 2004; Mohriak et al. 2008).

The study area is located in the salt-diapir domain (Fig. 2). Here, salt diapirs are rooted along two NW–SE-trending salt ridges (Fig. 2b of Gamboa and Alves 2015). These two ridges delimit a salt-withdrawal basin, within which the Rio Doce Canyon System was developed (Alves et al. 2009; Gamboa and Alves 2015). The relative location and movement of salt diapirs have a strong effect on the stratigraphic architecture of the study area, controlling the deposition of MTDs, turbidite lobes, and submarine canyons and channels (Baudon and Cartwright 2008; Alves et al. 2009; Gamboa et al. 2010; Gamboa et al. 2012; Gamboa and Alves 2015). For example, some of the observed MTDs were derived from the flanks of salt diapirs, i.e., they are detached MTDs associated with salt deformation (Omosanya and Alves 2013). Additionally, relatively high confinement imposed by the salt diapirs resulted in the development of a large confluence region in the study area, as shown by the clustering patterns of submarine channels recorded from the Miocene to the present day (Fig. 7 of Gamboa et al. 2012).

DATA AND METHODOLOGY

The interpreted seismic volume is located in the northern part of the Espírito Santo Basin, SE Brazil (Fig. 1A). This seismic volume was acquired by a dual airgun array and a 6×5700 m array of streamers. Bin size in this survey is 12.5 m by 12.5 m, with a 2 ms vertical sampling interval, resampled at 4 ms during stacking. Data processing included resampling, spherical divergence corrections, and zero-phase conversions undertaken before stacking, 3-D prestack time migration using the Stolt algorithm, and one-pass 3-D

migration. The dominant frequency of the data is 40 Hz. Time-depth conversions were made using P-wave velocities of 1480 m/s for the seafloor and 1600 m/s for strata studied in this work, just below the seafloor. The SEG standard was used in the seismic data, i.e., positive amplitude reflections (red) on the seismic profiles indicate an increase in acoustic impedance (Fig. 3).

The mapping of the Pliocene–Quaternary Rio Doce Channel System involved a combination of autotracking and manual line-by-line interpretation. Architectural elements in the channel system were imaged by selected seismic lines, combined with dip maps, root-mean-square (RMS) amplitude maps, thickness maps, and variance slices extracted from the interpreted seismic volume. Quantitative analyses were conducted along the main pathway (east tributary and post-confluence channel) of the channel system (Fig. 1B), with its width and height measured at 62.5 m intervals (Fig. 3). The width is the distance between the banks of the channel system (Fig. 3). The height is the distance between the bank and the deepest point of the channel system (Fig. 3). The cross-sectional area (CSA) of the channel system was measured at 1 km intervals (Fig. 3).

RESULTS

Seismic Facies

Four types of seismic facies were interpreted based on their seismic amplitude, reflection continuity, reflection geometry, and termination patterns against adjacent strata (Fig. 4). The interpretation of seismic facies was based on widely accepted criteria for deep-water settings (e.g., Posamentier and Kolla 2003; Mayall et al. 2006; Catterall et al. 2010; Deptuck et al. 2003; Janocko et al. 2013).

Seismic Facies 1 is characterized by high-amplitude, continuous to discontinuous seismic reflections (Fig. 4A), and is usually confined within V- or U-shaped erosional surfaces (Fig. 4B–E). This facies is interpreted as comprising the basal lags of submarine channels (e.g., Deptuck et al. 2003; Mayall et al. 2006; Catterall et al. 2010). It corresponds to coarse-grained sediments accumulated at the bases of submarine channels (e.g., McHargue and Webb 1986; Mayall et al. 2006).

Seismic Facies 2 consists of low- to high-amplitude, subparallel and continuous seismic reflections (Fig. 4A). This facies may have different origins: channel deposits accumulated in a channel-abandonment stage (e.g., Deptuck et al. 2003; Catterall et al. 2010; Janocko et al. 2013), or overbank deposits, some of which show a wedge-shaped geometry (Fig. 4B–E). These latter are interpreted as levee deposits (e.g., Posamentier and Kolla 2003; Deptuck et al. 2003; Catterall et al. 2010; Janocko et al. 2013).

Seismic Facies 3 is composed of variable-amplitude, chaotic, discontinuous seismic reflections (Fig. 4A). This facies represents mass-transport deposits (MTDs) and is attributed to processes such as slides, slumps, and debris flows (e.g., Posamentier and Kolla 2003; Mayall et al. 2006; Janocko et al. 2013). Blocks with high-amplitude, parallel reflections are observed in the MTDs (Fig. 4B, C).

Seismic Facies 4 is composed of low-amplitude, parallel, continuous seismic reflections interpreted as background hemipelagic sediment (Fig. 4).

General Morphology of the Pliocene–Quaternary Rio Doce Channel System

The Pliocene–Quaternary Rio Doce Channel System is a partly filled channel system (Qin et al. 2016). It is recognized as a sinuous channel on seismic data (Figs. 1B, 5). The morphology of the channel system varies across the continental slope (Figs. 5, 6).

Three main regions were established as a function of the topographic confinement imposed by salt diapirs (Fig. 5; Gamboa et al. 2012). In the pre-confluence region of lower confinement, the channel system is composed of two tributaries (Fig. 5). The west tributary shows initially a NNW–SSE course on the upper slope, shifting to a NW–SE strike at a water depth of ~ 1100 m. The east tributary shows a change in strike from NNE–SSW to NE–SW at a water depth of ~ 1300 m, due to the presence of salt diapir D5 (Fig. 5). An abandoned channel segment is identified in this same region (Fig. 5). The channel system is ~ 1000 m wide, and more than 200 m high in the pre-confluence region (Fig. 6A, B). The cross-sectional area (CSA) of the channel system ranges from 0.087 km² to 0.256 km² (Fig. 6C).

In the confluence region, where gravity flows tend to be deflected off the salt diapirs due to the higher degree of confinement imposed by these structures, the general orientation of the channel system changes to nearly N–S and is maintained toward the southernmost part of the study area (Fig. 5). The width, height, and CSA of the channel system increase rapidly in the confluence region (Fig. 6). The width of the channel system increases from ~ 1 km to 6 km. Its height increases ~ 50 m on average, and the CSA rises up to 1.2 km², which is 4 to 10 times larger than the CSA in other parts of the channel system (Fig. 6).

In the post-confluence region, the width and CSA of the channel system decrease significantly, from 6 km to 1–2 km and from 1.2 km² to ~ 0.2 km², respectively (Fig. 6A, B). The height of the channel system shows small changes compared to the confluence region (Fig. 6C).

Architectural Elements of the Channel System in the Confluence Region

The following sections of the paper focus on the channel system in the confluence region, where the channel system is widest and largest (Figs. 5, 6, 7).

In the confluence region, multiple erosional events are identified in the channel system (Fig. 8). Four main channel units, including three abandoned channels (Channels 1, 2a, and 2b), a channel belt (Channel 3), and an MTD are interpreted based on their seismic facies (Figs. 8E, 9).

Mass-Transport Deposit (MTD A).—This unit is chiefly composed of Seismic Facies 3 (Fig. 9C–H, K, L), and is interpreted as a locally sourced MTD, named MTD A herein. This deposit is located in a basal scar. The basal scar (or scar) in this study is defined as the erosional morphological feature within which MTD A was contained. The scar has a headwall, base, lateral margins, and toe area, all of which are associated with the headwall, base, lateral margins, and toe of MTD A (Figs. 9E, F, 10A).

MTD A was most likely frontally confined despite the fact that its frontal ramp is now eroded by Channel 2 (Fig. 9E, F). Because of confinement at the toe region, the MTD A was probably not transported downslope. The MTD is thus interpreted to have been formed by the mass-wasting event that created the scar, rather than being sourced from upslope regions.

A continuous, negative amplitude reflection underlies the chaotic facies in MTD A and is interpreted as the basal surface of the scar (Fig. 9C–H, K, L). However, no clear kinematic indicators of mass wasting were identified on the basal surface (Fig. 10A). The top surface of MTD A is a hummocky surface and shows traces of channel erosion (Fig. 10B). A stratified block is recognized in the chaotic reflections of MTD A (Fig. 9C, D). The block is 1 km long and 80 m thick and covers an area of 0.6 km². The orientation of the eastern margin of MTD A indicates that mass-wasting deposits, chiefly transported to the south, were confined upslope by salt diapir D5 and formed wider lobes downslope (Figs. 8E, 9E, F, 10A, B).

Based on the extent of MTD A, we can conclude that the headwall of the scar is 3 km wide (Fig. 8E) and at least 260 m high (Fig. 9E, F). The length of the scar is at least 8 km along its longitudinal direction (Fig. 9E, F). The eastern margin of the scar is 160–240 m high, and its width is at least 1 km (Fig. 9C, D). The estimated original volume of the scar is 1.6 km³. A scar of similar size has also been documented in Cambrian marine units in Canada, where the scar is at least 8 km long and 200 m high (Stewart et al. 1993).

Following the classification of Moscardelli and Wood (2008), MTD A is a detached MTD. Its formation is probably associated with salt deformation due to the spatial co-occurrence of the MTD and nearby salt diapir D5 (Fig. 8E). Moscardelli and Wood (2015) documented a relationship between the dimensions of MTDs and their origins. They show that detached MTDs are smaller than shelf- and slope-attached MTDs (Moscardelli and Wood 2015). The results of this work are consistent with the relationship observed by Moscardelli and Wood (2015), inasmuch as the area and length of MTD A plot into the area-length cluster of points for detached MTDs (Fig. 3 of Moscardelli and Wood 2015).

The presence of MTD A indicates a mass-wasting event that occurred in the confluence region, where the basal scar was later modified by subsequent channel erosion, as exemplified by the channel-fill deposits that overlie MTD A (Fig. 9C–H, K, L) and attribute maps for MTD A in Figure 10C and D.

The thickness of MTD A ranges from 8 m to 120 m (Fig. 10C), which is lower than the scar-margin height of 160–240 m (Fig. 9C, D, G, H). Such a difference suggests that part of MTD A has been removed downslope by turbidity flows. This removal is also supported by the thinner MTD A along the pathways of Channels 2b and 3 (Fig. 10C). Additionally, significant erosion of MTD A by channels is revealed by the variance slice extracted above the basal surface of MTD A (Fig. 10D). This slice shows that channel deposits of lower variance cut through the higher-variance MTD A (Fig. 10D).

Submarine Channels.—Three abandoned channels (Channels 1, 2a, and 2b) and a channel belt (Channel 3) have been interpreted inside the channel system in the

confluence region (Fig. 8E). These channels and channel belt comprise Seismic Facies 1 and 2 (Fig. 9).

Channel 1 is located on the western side of the channel system, being incised and overlain by Channel 3 (Figs. 8E, 9G–J). The height of Channel 1 is ~ 150 m with respect to its western bank. Its width increases from 550 up to 1200 m due to a sharp change from a straight to a scalloped bank (Fig. 8E) formed by localized bank failures.

Channel 2 is composed of two segments, identified as Channels 2a and 2b, which could have been connected as one single channel. Channel 2a occurs on the western side of the channel system and comprises an upper and a lower segment (Fig. 8E). The upper segment is relatively straight (Fig. 8E), and shows its erosional base only due to subsequent erosion by the west tributary of Channel 3 (Fig. 9A, B). This segment might be a paleo-pathway of the west tributary on the modern seafloor (Fig. 5). The upper segment of Channel 2a is ~ 120 m high with a 100–200 m wide thalweg (Fig. 9A, B). The lower segment of Channel 2a is incised by Channel 3 to the east and shows a scalloped bank to the west (Fig. 8E). This segment is 150 m high and 800 m wide (Fig. 9C, D). The scalloped bank in this segment is interpreted to be a result of bank failure, which widened the base of the channel from 100 m to a maximum of 700 m (Fig. 9C, D).

Channel 2b is located on the eastern side of the channel system, being 1000 m wide and 150 m high (Figs. 8E, 9G, H, K, L). It incises MTD A in two parts and shows a relatively sinuous pathway, with sinuosity approaching 1.7 (Fig. 8E). Channel 2b is itself incised and overlain by Channel 3 (Figs. 8E, 9E–H, K, L).

Channel 3 is a channel belt marked by lateral channel migration, as revealed by abrupt shifts in channel forms (Fig. 9C, D, G, H; Fig. 13 of Qin et al. 2016). Channel 3 has two tributaries and a post-confluence channel on the seafloor (Fig. 5). It is 1000–2000 m wide by 140–180 m high in the confluence region. This channel is traceable throughout the entire seismic volume and incises all the other erosional features, including Channels 1, 2 and MTD A (Fig. 8E). It also shows well-developed levees above both MTD A and sediment fills of other channels (Fig. 9C, D, G–J).

Surface E.—Surface E is a high-amplitude, negative reflection that is interpreted throughout the study area (Figs. 9C–L, 11A). Part of Surface E was used as the basal erosional surface of MTD A (Fig. 9C–H, K, L). The thickness between Surface E and the basal erosional surfaces of channels (Channels 1 and 3, part of Channel 2) ranges from 0 to 10 ms (Fig. 11B). These low thickness values suggest that Surface E played a key role in delimiting the erosional base of both the channels and MTD A. Surface E is probably a mechanically weak layer acting as a detachment surface, above which mass wasting tends to occur. However, the lithology of this surface is unknown due to the lack of well data in the study area.

DISCUSSION

Depletion Zone of the Basal Scar and Flow Capture

Seismic data show that the enlargement of the channel system in the confluence region resulted mainly from the spatial co-occurrence of MTD A and Channels 1 and 2 (Fig. 8E). This character indicates that important interactions between MTDs and turbidity flows occurred in the confluence region. Such interactions are suggested to have started with flow-capture processes.

Turbidity flows can be captured by depletion zones on the headwall domains of basal scars (Shultz et al. 2005; Kertznus 2009; Kneller et al. 2016), where bathymetric lows are developed due to sediment evacuation and local extension (e.g., Lewis 1971; Martinsen and Bakken 1990; Frey Martinez et al. 2005; Bull et al. 2009). These same phenomena are exemplified in the Gulf of Mexico and the Nile Delta continental slope, where channels have been captured by the headwalls of basal scars (Hackbarth and Shew 1994; Winker and Booth 2000; Loncke et al. 2009; Kertznus 2009; Kneller et al. 2016).

In the study area, part of the depletion zone is presently filled by channel-fill deposits, but there is still a topographic low downslope of the headwall of the scar (Figs. 9E, F, 12A). Upslope from the headwall, a channel segment (Channel A) has been identified (Fig. 12A). The path of Channel A connects to the headwall of the scar (Fig. 12A), suggesting that turbidity flows are still captured by the scar at present. In addition, a set of NW–SE-trending grooves are observed upslope of the headwall (Fig. 12). These grooves can be tracked to a channel (Channel B) where bank failure occurred (Fig. 12A, B). Because submarine channels are flushed by turbidity flows, the grooves are thus believed to have been formed by sheet turbidity flows that breached the bank of Channel B. Despite the lack of temporal constraints for their genesis, the presence of grooves on the seafloor suggests that unconfined sheet flows may have been captured by the headwall of the basal scar.

Channels 1, 2, and 3 are interpreted to reflect different episodes of flow-capture processes (Fig. 13). After the basal scar was generated, it captured turbidity flows at its headwall (Fig. 13A, B) and these captured flows removed part of MTD A along the longitudinal direction (N–S) of the scar (Fig. 13B). Channel 1 should have been formed at this stage (Fig. 13B), because its bank orientation is similar to the longitudinal direction (N–S) of MTD A (Fig. 8E). Erosion along the longitudinal direction (N–S) of MTD A enlarged the depletion zone of the scar (Fig. 13B), and allowed flow capture at its west margin, as shown by the presence of Channel 2 (Fig. 13C). Channel 3 is believed to have been captured by the headwall of the scar, based on its position with respect to the scar (Fig. 13D).

Compared to shelf-edge scars recognized in the Gulf of Mexico (Winker and Booth 2000; Kneller et al. 2016) and the Nile Delta slope (Kertznus 2009), which incise the shelf break and connect shelf-edge deltas with upper-slope depositional systems (Kneller et al. 2016), we present a case study of flow capture in a different slope setting. In this work, the basal scar is located in a confluence region confined by salt diapirs (Fig. 13A). Therefore, turbidity flows derived from source areas upslope tend to be deflected into the basal scar due to the presence of salt diapirs (Figs. 5, 13A). Flow deflection caused by salt diapirs increases the probability of flow-capture processes, which might have been frequent throughout the evolution of the channel system. For example, adding to flow capture in the headwall region of the scar shown by the presence of Channels 1, 3, and A

(Fig. 13B, D), this paper exemplifies a flow-capture pattern that has not been documented in previous work. The relative positions of Channel 2 and adjacent basal scar (Figs. 8E, 13C) suggest that turbidity flows could also be captured by the lateral margins of scars. Such a capture process resulted mainly from flow deflection due to the presence of the confluence region created by the salt diapirs (Fig. 13A).

A Mechanism for Channel Initiation

Flow confinement is an important process in channel initiation, and can be achieved by channel incision and levee construction (e.g., Straub and Mohrig 2009; Rowland et al. 2010; Weill et al. 2014; De Leeuw et al. 2016). In addition to these studies, we suggest that flow confinement and channelization also result from flow-capture processes. On the seafloor, erosional grooves generated by unconfined flows are observed upslope of the scar (Fig. 12), indicating that sheet turbidity flows were funnelled into the scar. This process forced the unconfined sheet flows into a confined flow, thus enhancing flow channelization in the study area.

Large slope valleys have been suggested to be formed at the early stage of channel formation, with MTDs at their bases (e.g., Samuel et al. 2003; Mayall et al. 2006; Macauley and Hubbard 2013). As mass-wasting events can be precursors of submarine channels, some of these valleys may be filled by debris-flow deposits and later modified by subsequent turbidity flows, which are able to erode MTDs on the continental slope and deposit channel-fill deposits in the scars (Fig. 13).

Interaction between MTDs and Turbidity Flows

Morphological Changes in the Basal Scar.—The basal scar is interpreted as having been widened on its western margin (Fig. 9C, D, G, H). The presence of scalloped banks in Channels 1 and 2a (Fig. 8E) highlights the role of localized mass failures in the widening of the scar. The generation of these scalloped banks is attributed to small-scale sediment failure triggered by turbidity flows.

The lateral continuity of Surface E indicates that most erosional processes occurred above this specific surface (Fig. 9C–L). Such an erosional pattern suggests that the interval between the deposition of MTD A and subsequent channel erosion may have been so short that they preceded the consolidation of MTD A. Therefore, MTD A was weaker than the strata beneath Surface E, and, as a result, turbidity flows preferentially eroded the more friable MTD A above Surface E rather than incising downward into older deposits. This process resulted in a pronounced widening of the basal scar with small change in its height (Fig. 9C–H, K, L).

Differences in sediment strength within and outside of the scar also influence the pathways of channels. For instance, Channel 2b probably used the margin of the basal scar as its east bank (Fig. 8E), thus focusing erosion in areas where MTD A was present (Figs. 8E, 9E–H). A similar process occurred in the eastern Gulf of Mexico, where the east bank of the Einstein channel system was constrained by the eastern margin of a basal scar (Fig. 11 of Kneller et al. 2016). Such a spatial association between the margins of

channel systems and basal scars suggests that turbidity flows tend to erode less resistant MTDs within the scars rather than more resistant sediments outside them.

Replacement of Strata in the Basal Scar, and Reservoir Implications.—Along the course of Channel 2b, a large volume of MTD A was removed and replaced by sand-prone channel-fill deposits (Fig. 9E–H, K, L). As a result of such erosion, the thickness of MTD A ranges from 8 m to 40 m along Channel 2b, where is thinnest, whereas the remainder of MTD A is 40 m to 120 m thick (Fig. 10C).

Additionally, the thickness variations in MTD A indicate that differential erosion occurred in this MTD, especially along the east margin of the scar and the pathway of Channel 2b (Fig. 10C). This erosional pattern may have resulted from variations in the properties of turbidity flows. The thicker MTD interval along the longitudinal direction (N–S) of the scar may have been affected by less erosive and less frequent flows captured by the headwall. Conversely, the thinner MTD interval along Channel 2b indicates more erosive and more frequent turbidity flows captured by the western margin of the scar.

Although MTDs are generally considered as poor reservoirs due to their low porosity and permeability (Posamentier and Kolla 2003; Moscardelli et al. 2006), their associated depositional systems, especially submarine channels and lobes, are recognized as important hydrocarbon reservoirs in deep-water settings (Mayall et al. 2006; Armitage et al. 2009; Jackson and Johnson 2009; Kneller et al. 2016). This work shows that the erosion and replacement of strata above basal scars increased reservoir potential by the continuous obliteration of pre-existing MTDs in scars. This process enhanced the lateral continuity of turbidites and limited the local compartmentalization of sandy reservoir intervals by MTDs (Mayall et al. 2006; Moscardelli et al. 2006).

CONCLUSIONS

This study used 3D seismic data to document how mass wasting influenced the geometry and distribution of subsequent submarine channels, as well as the replacement of MTDs by channel-fill deposits. In summary:

- In a confluence region confined by salt diapirs, the Pliocene–Quaternary Rio Doce Channel System is wider and larger than other parts of channel system. An MTD, three abandoned channels, and a channel belt are identified in the channel system in the confluence region. These morphological and architectural features are interpreted to result from the interaction between mass-wasting deposits and subsequent turbidity flows.
- After a basal scar was generated by a mass-wasting event, it was used as a preferential pathway for subsequent turbidity flows, which were captured by the headwall and lateral margins of the scar.
- The morphology of the scar was modified by subsequent turbidity flows. The scar was greatly widened, with a small change in height, because of differences in sediment strength within and outside of the scar. In other words, the presence of softer MTDs hindered the downward incision of

turbidity flows which, instead, widened the scar laterally. This process resulted in a much wider channel system than expected in the confluence region.

- Basal scars formed by mass-wasting events can provide flow confinement and facilitate flow channelization, which are key processes for submarine-channel initiation.
- This work shows that the replacement of MTDs by channel-fill deposits was achieved through multiple cut-and-fill episodes associated with turbidity flows captured by the scar. An MTD with poor reservoir quality was replaced by channel-fill deposits of higher reservoir potential. Such replacement and associated reservoir potential relate to the properties of turbidity flows, such as their erosive ability and frequency.

ACKNOWLEDGMENTS

The authors acknowledge the permission conceded by CGG for the publication of this research paper. Davide Gamboa publishes with the permission of the Executive Director, British Geological Survey, and thanks the National Research Network for Low Carbon, Energy and the Environment (NRN-LCEE) for research support. Associate editor Dr. Morgan Sullivan, Dr. Lorena Moscardelli, and Dr. Tim McHargue are acknowledged for their constructive comments.

REFERENCES

- Abdurrokhim, and Ito, M., 2013, The role of slump scars in slope channel initiation: a case study from the Miocene Jatiluhur Formation in the Bogor Trough, West Java: *Journal of Asian Earth Sciences*, v. 73, p. 68–86.
- Alves, T.M., 2010, 3D Seismic examples of differential compaction in mass-transport deposits and their effect on post-failure strata: *Marine Geology*, v. 271, p. 212–224.
- Alves, T.M., 2012, Scale-relationships and geometry of normal faults reactivated during gravitational gliding of Albian rafts (Espírito Santo Basin, SE Brazil): *Earth and Planetary Science Letters*, v. 331–332, p. 80–96.
- Alves, T.M., Cartwright, J., and Davies, R.J., 2009, Faulting of salt-withdrawal basins during early halokinesis: effects on the Paleogene Rio Doce Canyon system (Espírito Santo Basin, Brazil): *American Association of Petroleum Geologists, Bulletin*, v. 93, p. 617–652.
- Armitage, D.A., Romans, B.W., Covault, J.A., and Graham, S.A., 2009, The influence of mass transport deposit surface topography on the evolution of turbidite architecture: the Sierra Contreras, Tres Pasos Formation (Cretaceous), southern Chile: *Journal of Sedimentary Research*, v. 79, p. 287–301.
- Bain, H.A., and Hubbard, S.M., 2016, Stratigraphic evolution of a long-lived submarine channel system in the Late Cretaceous Nanaimo Group, British Columbia, Canada: *Sedimentary Geology*, v. 337, p. 113–132.

- Baudon, C., and Cartwright, J., 2008, The kinematics of reactivation of normal faults using high resolution throw mapping: *Journal of Structural Geology*, v. 30, p. 1072–1084.
- Bernhardt, A., Stright, L., and Lowe, D.R., 2012, Channelized debris-flow deposits and their impact on turbidity currents: the Puchkirchen axial channel belt in the Austrian Molasse Basin: *Sedimentology*, v. 59, p. 2042–2070.
- Bruhn, C.H.L., and Walker, R.G., 1997, Internal architecture and sedimentary evolution of coarse-grained, turbidite channel–levee complexes, early Eocene Regência canyon, Espírito Santo Basin, Brazil: *Sedimentology*, v. 44, p. 17–46.
- Bull, S., Cartwright, J., and Huuse, M., 2009, A review of kinematic indicators from mass-transport complexes using 3D seismic data: *Marine and Petroleum Geology*, v. 26, p. 1132–1151.
- Catterall, V., Redfern, J., Gawthorpe, R., Hansen, D., and Thomas, M., 2010, Architectural style and quantification of a submarine channel–levee system located in a structurally complex area: offshore Nile Delta: *Journal of Sedimentary Research*, v. 80, p. 991–1017.
- Chang, H.K., Kowsmann, R.O., Figueiredo, A.M., and Bender, A.A., 1992, Tectonics and stratigraphy of the East Brazil Rift system: an overview: *Tectonophysics*, v. 213, p. 97–138.
- Cobbold, P.R., Meisling, K.E., and Mount, V.S., 2001, Reactivation of an obliquely rifted margin, Campos and Santos basins, southeastern Brazil: *American Association of Petroleum Geologists, Bulletin*, v. 85, p. 1925–1944.
- Cordani, U.G., 1970, Idade do vulcanismo no Oceano Atlântico Sul: *Universidade de São Paulo, Instituto de Geociências e Astronomia, Boletim*, 94 p.
- Corella, J.P., Loizeau, J.L., Kremer, K., Hilbe, M., Gerard, J., Le Dantec, N., Stark, N., González-Quijano, M. and Giradclos, S., 2016, The role of mass-transport deposits and turbidites in shaping modern lacustrine deepwater channels: *Marine and Petroleum Geology*, v. 77, p. 515–525.
- Davison, I., 1999, Tectonics and hydrocarbon distribution along the Brazilian South Atlantic margin, *in* Cameron, N.R., Bate R.H., and Clure V.S., eds., *The Oil and Gas Habitats of the South Atlantic: Geological Society of London, Special Publication 153*, p. 133–151.
- De Leeuw, J., Eggenhuisen, J.T., and Cartigny, M.J.B., 2016, Morphodynamics of submarine channel inception revealed by new experimental approach: *Nature Communications*, v. 7, p. 1–7.
- Demercian, S., Szatmari, P., and Cobbold, P.R., 1993, Style and pattern of salt diapirs due to thin-skinned gravitational gliding, Campos and Santos basins, offshore Brazil: *Tectonophysics*, v. 228, p. 393–433.
- Deptuck, M.E., Steffens, G.S., Barton, M., and Pirmez, C., 2003, Architecture and evolution of upper fan channel-belts on the Niger Delta slope and in the Arabian Sea: *Marine and Petroleum Geology*, v. 20, p. 649–676.
- Eggenhuisen, J.T., McCaffrey, W.D., Haughton, P.D.W., Butler, R.W.H., Moore, I., Jarvie, A., and Hakes, W.G., 2010, Reconstructing large-scale remobilisation of deep-water deposits and its impact on sand-body architecture from cored wells: the

- Lower Cretaceous Britannia Sandstone Formation, UK North Sea: *Marine and Petroleum Geology*, v. 27, p. 1595–1615.
- Fiduk, J.C., Brush, E.R., Anderson, L.E., Gibbs, P.B., and Rowan, M.G., 2004, Salt deformation, magmatism, and hydrocarbon prospectivity in the Espírito Santo Basin, offshore Brazil, *in* Post, P.J., Olson, D.L., Lyons, K.T., Palmes, S.L., Harison, P.F., and Rosen, N.C., eds., *Salt-Sediment Interactions and Hydrocarbon Prospectivity: Concepts, Applications, and Case Studies for the 21st Century*: SEPM, Gulf Coast Section, 24th Annual Research Conference, p. 370–392.
- Frey Martinez, J., Cartwright, J., and Hall, B., 2005, 3D seismic interpretation of slump complexes: examples from the continental margin of Israel: *Basin Research*, v. 17, p. 83–108.
- Gamboa, D., and Alves, T.M., 2015, Spatial and dimensional relationships of submarine slope architectural elements: a seismic-scale analysis from the Espírito Santo Basin (SE Brazil): *Marine and Petroleum Geology*, v. 64, p. 43–57.
- Gamboa, D., Alves, T.M., and Cartwright, J., 2012, A submarine channel confluence classification for topographically confined slopes: *Marine and Petroleum Geology*, v. 35, p. 176–189.
- Gamboa, D., Alves, T., Cartwright, J., and Terrinha, P., 2010, MTD distribution on a “passive” continental margin: the Espírito Santo Basin (SE Brazil) during the Palaeogene: *Marine and Petroleum Geology*, v. 27, p. 1311–1324.
- Gee, M.J.R., Gawthorpe, R.L., Bakke, K., and Friedmann, S.J., 2007, Seismic geomorphology and evolution of submarine channels from the Angolan continental margin: *Journal of Sedimentary Research*, v. 77, p. 433–446.
- Hackbarth, C.J., and Shew, R.D., 1994, Morphology and stratigraphy of a mid Pleistocene turbidite leveed channel from seismic, core, and log data, *in* Bouma, A.H., Weimer, P., and Perkins, B., eds., *Submarine Fans and Turbidite Systems*: SEPM, Gulf Coast Section, 15th Annual Research Conference, p. 127–133.
- Hampton, M.A., Lee, H.J., and Locat, J., 1996, Submarine landslides: Review of Geophysics, v. 34, p. 33–59.
- Hansen, L., L’Heureux, J.S., Sauvin, G., Polom, G., Lecomte, I., Vaneste, M., Longva, O., and Krawczyk, C., 2013, The effect of mass-wasting on the stratigraphic architecture of a fjord-valley fill: correlation of onshore, shear wave seismics and marine seismic data at Trondheim, Norway: *Sedimentary Geology*, v. 289, p. 1–18.
- Jackson, C.A.L., and Johnson, H.D., 2009, Sustained turbidity currents and their interaction with debrite-related topography: Labuan Island, offshore NW Borneo, Malaysia: *Sedimentary Geology*, v. 219, p. 77–96.
- Janocko, M., Nemec, W., Henriksen S., and Warcho, M., 2013, The diversity of deep-water sinuous channel belts and slope valley-fill complexes: *Marine and Petroleum Geology*, v. 41, p. 7–34.
- Joanne, C., Collot, J.-Y., Lamarche, G., and Migeon, S., 2010, Continental slope reconstruction after a giant mass failure, the example of the Matakaoa margin, New Zealand: *Marine Geology*, v. 268, p. 67–84.
- Kertzus, V., 2009, *Stratigraphic Development of Delta-Fed Slope Systems: Offshore Ebro and Nile Deltas* [Ph.D. thesis]: University of Aberdeen, 298 p.

- Kneller, B., and McCaffrey, W., 1999, Depositional effects of flow nonuniformity and stratification within turbidity currents approaching a bounding slope: deflection, reflection, and facies variations: *Journal of Sedimentary Research*, v. 69, p. 980–991.
- Kneller, B., Dykstra, M., Fairweather, L., and Milana, J.P., 2016, Mass-transport and slope accommodation: implications for turbidite sandstone reservoirs: *American Association of Petroleum Geologists, Bulletin*, v. 100, p. 213–235.
- Lewis, K.B., 1971, Slumping on a continental slope inclined at 1–4°: *Sedimentology*, v. 16, p. 97–110.
- Lucente, C.C., and Pini, G.A., 2008, Basin-wide mass-wasting complexes as markers of the Oligo-Miocene foredeep-accretionary wedge evolution in the Northern Apennines, Italy: *Basin Research*, v. 20, p. 49–71.
- Loncke, L., Gaullier, V., Droz, L., Ducassou, E., Migeon, S., and Mascle, J., 2009, Multi-scale slope instabilities along the Nile deep-sea fan, Egyptian margin: a general overview: *Marine and Petroleum Geology*, v. 26, p. 633–646.
- Macauley, R.V., and Hubbard, S.M., 2013, Slope channel sedimentary processes and stratigraphic stacking, Cretaceous Tres Pasos Formation slope system, Chilean Patagonia: *Marine and Petroleum Geology*, v. 41, p. 146–162.
- Martinsen, O.J., and Bakken, B., 1990, Extensional and compressional zones in slumps and slides in the Namurian of County Clare, Ireland: *Geological Society of London, Journal*, v. 147, p. 153–164.
- Masalimova, L., Lowe, D.R., McHargue, T., and Derksen, R., 2015, Interplay between an axial channel belt, slope gullies and overbank deposition in the Puchkirchen Formation in the Molasse Basin, Austria: *Sedimentology*, v. 62, p. 1717–1748.
- Mayall, M., Jones, E., and Casey, M., 2006, Turbidite channel reservoirs: key elements in facies prediction and effective development: *Marine and Petroleum Geology*, v. 23, p. 821–841.
- McAdoo, B.G., Pratson, L.F., and Orange, D.L., 2000, Submarine landslide geomorphology, U.S. continental slope: *Marine Geology*, v. 169, p. 103–136.
- McHargue, T.R., and Webb, J.E., 1986, Internal geometry, seismic facies, and petroleum potential of canyons and inner fan channels of the Indus submarine fan: *American Association of Petroleum Geologists, Bulletin*, v. 70, p. 161–180.
- Mohriak, W.U., 2003, Bacias sedimentares da margem continental Brasileira, *in* Bizzi, L.A., Schobbenhaus, C., Vidotti, R.M., and Goncalves, J.H., eds., *Geologia, Tectonica e Recursos Minerais do Brasil: Companhia de Pesquisa Recursos Minerais*, Brasilia, p. 87–165.
- Mohriak, W.U., 2005, Interpretação geológica e geofísica da Bacia do Espírito Santo e da região de Abrolhos: petrografia, datação radiométrica e visualização sísmica das rochas vulcânicas: *Boletim de Geociências da Petrobras*, v. 14, p. 133–142.
- Mohriak, W.U., Nemcok, M., and Enciso, G., 2008, South Atlantic divergent margin evolution: rift-border uplift and salt tectonics in the basins of Southeastern Brazil, *in* Pankhurst, R.J., Trouw, R.A.J., Brito Neves, B.B., De Wit, M.J., eds., *West Gondwana Pre-Cenozoic Correlations across the South Atlantic Region: Geological Society of London, Special Publication 294*, p. 365–398.

- Moscardelli, L., and Wood, L., 2008, New classification system for mass transport complexes in offshore Trinidad: *Basin Research*, v. 20, p. 73–98.
- Moscardelli, L., and Wood, L., 2015, Morphometry of mass transport deposits as a predictive tool: *Geological Society of America, Bulletin*, v. 128, p. 47–30.
- Moscardelli, L., Wood, L., and Mann, P., 2006, Mass-transport complexes and associated processes in the offshore area of Trinidad and Venezuela: *American Association of Petroleum Geologists, Bulletin*, v. 90, p. 1059–1088.
- Ojeda, H.A.O., 1982, Structural framework, stratigraphy, and evolution of Brazilian marginal basins: *American Association of Petroleum Geologists, Bulletin*, v. 66, p. 732–749.
- Olafiranye, K., Jackson, C.A.-L., and Hodgson, D.M., 2013, The role of tectonics and mass-transport complex emplacement on upper slope stratigraphic evolution: a 3D seismic case study from offshore Angola: *Marine and Petroleum Geology*, v. 44, p. 196–216.
- Omosanya, K.O., and Alves, T.M., 2013, A 3-dimensional seismic method to assess the provenance of Mass-Transport Deposits (MTDs) on salt-rich continental slopes (Espírito Santo Basin, SE Brazil): *Marine and Petroleum Geology*, v. 44, p. 223–239.
- Ortiz-Karpf, A., Hodgson, D.M., and McCaffrey, W.D., 2015, The role of mass-transport complexes in controlling channel avulsion and the subsequent sediment dispersal patterns on an active margin: The Magdalena Fan, offshore Colombia: *Marine and Petroleum Geology*, v. 64, p. 58–75.
- Pickering, K.T., and Corregidor, J., 2005, Mass-transport complexes and tectonic control on confined basin-floor submarine fans, middle Eocene, south Spanish Pyrenees, *in* Hodgson, D.M., and Flint, S.S., eds., *Submarine Slope Systems: Processes and Products*: Geological Society of London, Special Publication 244, p. 51–74.
- Posamentier, H.W., and Kolla, V., 2003, Seismic geomorphology and stratigraphy of depositional elements in deep-water settings: *Journal of Sedimentary Research*, v. 73, p. 367–388.
- Qin, Y., Alves, T.M., Constantine, J., and Gamboa, D., 2016, Quantitative seismic geomorphology of a submarine channel system in SE Brazil (Espírito Santo Basin): scale comparison with other submarine channel systems: *Marine and Petroleum Geology*, v. 78, p. 455–473.
- Rowland, J.C., Hilley, G.E., and Fildani, A., 2010, A test of initiation of submarine leveed channels by deposition alone: *Journal of Sedimentary Research*, v. 80, p. 710–727.
- Samuel, A., Kneller, B., Raslan, S., Sharp, A., and Parsons, C., 2003, Prolific deep-marine slope channels of the Nile Delta, Egypt: *American Association of Petroleum Geologists, Bulletin*, v. 87, p. 541–560.
- Shultz, M.R., Fildani, A., Cope, T.D., and Graham, S.A., 2005, Deposition and stratigraphic architecture of an outcropping ancient slope system: Tres Pasos Formation, Magallanes Basin, southern Chile, *in* Hodgson, D.M., and Flint, S.S., eds., *Submarine Slope Systems: Processes and Products*: Geological Society of London, Special Publication 244, p. 27–50.

- Stewart, W.D., Dixon, O.A., and Rust, B.R., 1993, Middle Cambrian carbonate-platform collapse, southeastern Canadian Rocky Mountains: *Geology*, v. 21, p. 687–690.
- Straub, K.M., and Mohrig, D., 2009, Constructional canyons built by sheet-like turbidity currents: observations from offshore Brunei Darussalam: *Journal of Sedimentary Research*, v. 79, p. 24–93.
- Stright, L., Bernhardt, A., and Boucher, A., 2013, DFTopoSim: modeling topographically-controlled deposition of subseismic scale sandstone packages within a mass transport dominated deep-water channel belt: *Mathematical Geosciences*, v. 45, p. 277–296.
- Turner, O.C., 2015, Depositional Framework and Controls on Coeval Deep-Water Slope Channel and Slope Fan Systems in the Eocene Juncal formation, Southern California [Ph.D. thesis]: Colorado School of Mines, 129 p.
- Weill, P., Lajeunesse, E., and Devauchelle, O., 2014, Experimental investigation on self-channelized erosive gravity currents: *Journal of Sedimentary Research*, v. 84, p. 487–498.
- Winker, C.D., and Booth, J.R., 2000, Sedimentary dynamics of the salt-dominated continental slope, Gulf of Mexico: integration of observations from the seafloor, near surface and deep subsurface, *in* Weimer, P., Slatt, R.M., Coleman, J., Rosen, N.C., Nelson, H., Bouma, A.H., Styzen, M.J., and Lawrence, D.T., eds., *Deep-Water Reservoirs of the World: SEPM, Gulf Coast Section, 20th Annual Research Conference*, p. 1059–1086.

Received 21 September 2016; accepted 25 January 2017.

FIGURE CAPTIONS

FIG. 1.—**A)** Regional map of the southeast Brazilian Margin showing the location of the interpreted seismic volume (see black square) in the Espírito Santo Basin. **B)** Contoured seafloor map of the study area extracted from 3D seismic data. D1 to D6 show the location of salt diapirs in the study area.

FIG. 2.—Simplified regional cross section across the Espírito Santo Basin, showing key variations in salt-deformation styles, from salt rollers and rafts in the proximal domain, salt diapirs in the transitional domain, to salt overhangs in the distal domain (Modified from Fiduk et al. 2004 and Gamboa et al. 2010). The location of the study area is highlighted by the black box.

FIG. 3.—Schematic diagram showing the morphological parameters used in the quantitative analyses of the Pliocene–Quaternary Rio Doce Channel System, including the width, height, and cross-sectional area of the channel system. **A)** Uninterpreted cross section of the channel system. **B)** Interpreted cross section of the channel system with parameters used in quantitative analyses.

FIG. 4.—**A)** Description and interpretation of seismic facies observed in the channel system. **B, C, D, E)** Uninterpreted and interpreted seismic sections highlighting the seismic facies interpreted in the channel system.

FIG. 5.—Schematic representation of seafloor geomorphologic features in the study area. The pre-confluence and confluence regions show a variety of erosional features such as irregular depressions, gullies, channels, and headwalls of mass-transport deposits (MTDs). In contrast, the post-confluence region is relative smooth around the Pliocene–Quaternary Rio Doce Channel System. The channel system is partially filled with sediment and shows multiple seafloor channels in it. These seafloor channels comprise west and east tributaries upslope, and a post-confluence channel downslope.

FIG. 6.—Quantitative analyses of the Pliocene–Quaternary Rio Doce Channel System (gray area in Fig. 5). The channel system is much larger in the confluence region than farther upslope (i.e., pre-confluence region) and downslope (i.e., post-confluence region). **A)** Width profile of the channel system. **B)** Height profile of the channel system. **C)** Variations in the cross-sectional area (CSA) of the channel system.

FIG. 7.—**A)** Dip map of the channel system in the confluence region. The location of cross sections in Figure 9 are shown in this figure. **B)** Basal erosional surface of the channel system in the confluence region. The base of the channel is much wider here than in both the pre- and post-confluence regions.

FIG. 8.—Architectural elements of the studied channel system in the confluence region. **A, B)** Uninterpreted and interpreted variance slices acquired 60 ms above Surface E, which is shown in Figure 9. They were extracted from a seismic volume flattened on Surface E. The dark irregular pattern represents chaotic MTDs, and the light colors represent channel-fill deposits. **C, D)** Uninterpreted and interpreted root-mean-square (RMS) amplitude maps acquired 65 ms above Surface E, which is shown in Figure 9. They are extracted from a flattened seismic volume based on Surface E. The irregular amplitude reflects the presence of chaotic MTDs. The RMS amplitude of channel-fill deposits ranges from low to high. **E)** Schematic diagram showing and naming architectural elements of the channel system in the confluence region, including three abandoned channels (Channels 1, 2a, and 2b), a channel belt (Channel 3), and MTD A. Channels 2a and 2b are interpreted as comprising a single channel.

FIG. 9.—Selected seismic sections (left-hand side) and their corresponding interpretations (right-hand side) highlighting the key architectural elements of the channel system in the confluence region. The location of seismic sections is shown in Figure 7A.

FIG. 10.—**A)** Time-structure map of the basal erosional surface of MTD A. **B)** Time-structure map of the top surface of MTD A. **C)** Thickness map of MTD A. The maximum thickness of MTD A is observed along its eastern margin, reaching approximately 120 m. The thickness of MTD A is much smaller where Channel 2b cuts through; it ranges from

8 to 40 m. **D)** Variance slice extracted 55 ms above the base of MTD A. The dark irregular pattern represents chaotic MTDs, and the light colors represent channel-fill deposits.

FIG. 11.—**A)** Time-structure map of Surface E. **B)** Thickness map between the basal erosional surfaces of erosional events (i.e., MTD A and channels) and Surface E. The thickness between the basal surface of MTD A and Surface E is 0 ms, whereas the thickness between the erosional surface of the channels and Surface E varies from 0 to 10 ms, suggesting that MTD A and adjacent channels (Channel 1, part of Channels 2 and 3) share the same erosional surface.

FIG. 12.—**A)** 3D view of seafloor morphology showing grooves upslope of the headwall of the scar. **B)** 2D view of seafloor morphology showing the grooves can be tracked to the bank of a channel (Channel B) where bank failures occurred. This character suggests that the grooves were formed by sheet turbidity flows that breached a channel bank. **C)** Seismic section showing a series of grooves on the seafloor.

FIG. 13.—Schematic diagram summarizing the evolution model of the channel system in the confluence region. D1 to D6 show the location of salt diapirs. **A)** Schematic diagram showing that the occurrence of a mass-wasting process in a confluence region confined by salt diapirs. A basal scar was created and was filled with MTD A. **B)** Schematic diagram showing that turbidity flows were captured by the headwall of the scar; these flows removed the upper part of MTD A downslope. Channel 1 was formed at this stage. **C)** Schematic diagram showing the stage in which Channel 2 was captured by the western wall of the scar. Channel 2 used the eastern margin of the scar as its bank. **D)** Schematic diagram showing that Channel 3 was captured by the headwall of the scar. This channel incised the toe of the scar and extends downslope toward the continental rise.

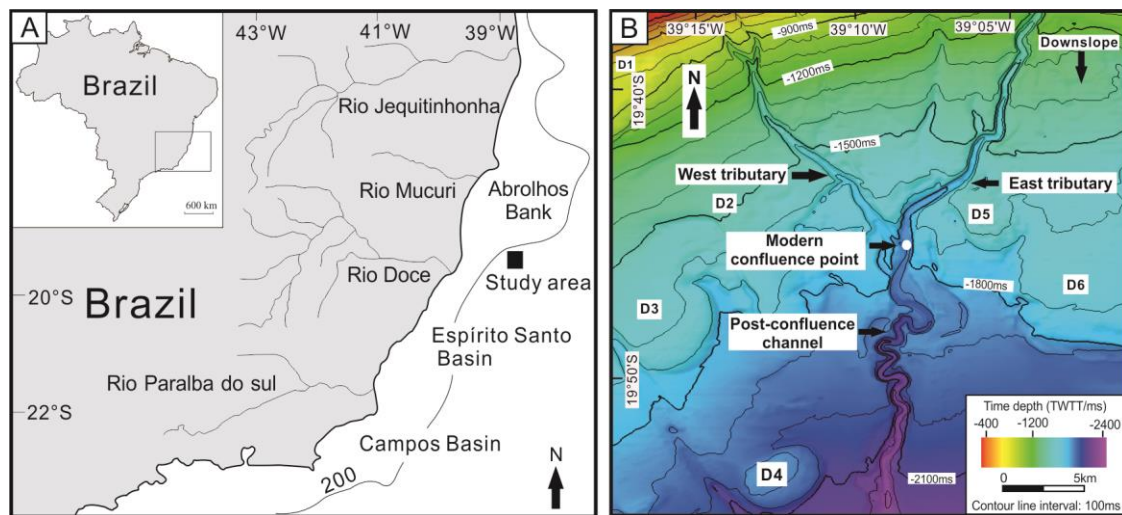


Figure 1

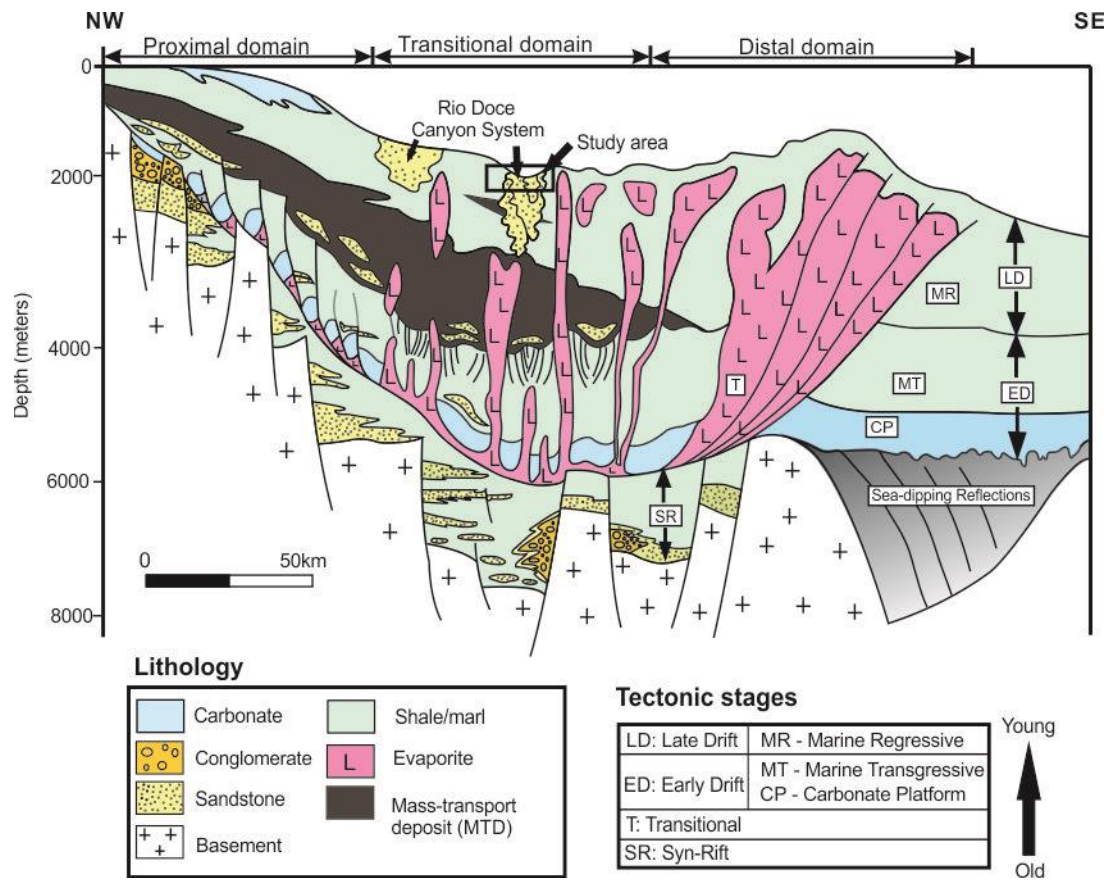


Figure 2

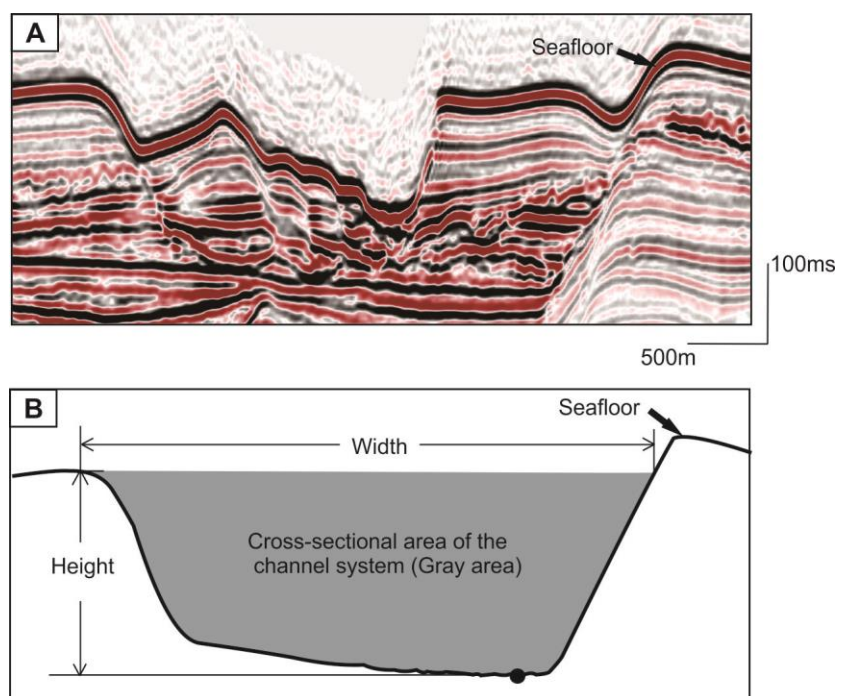

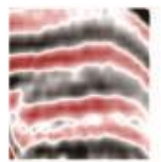
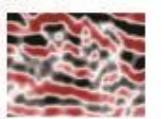



Figure 3

A	Seismic facies	Discription	Interpretation
1		High amplitude, continuous to discontinuous seismic reflections, usually confined within a V- or U- shaped erosional surface	Basal lags of channels
2		Low to high amplitude, parallel to sub-parallel, continuous reflections	Channel-fill deposits
3		Variable amplitude, chaotic, discontinuous reflections	Mass-transport deposits (MTDs)
4		Low amplitude, parallel, continuous reflections	Hemipelagic deposits

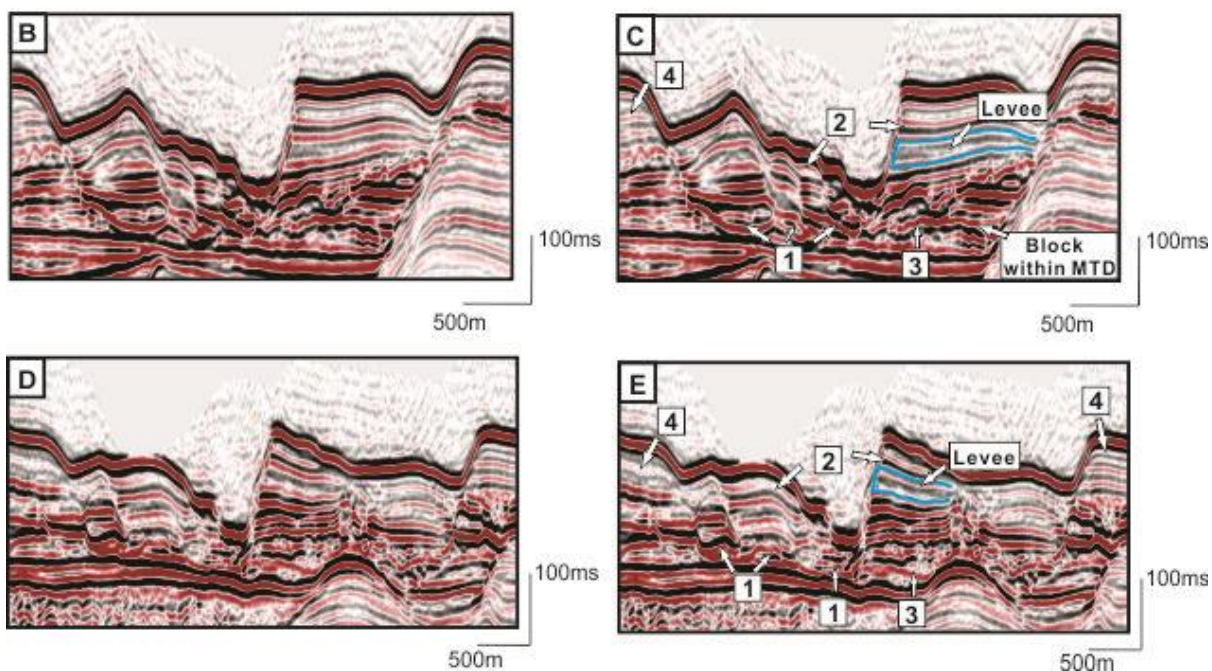


Figure 4

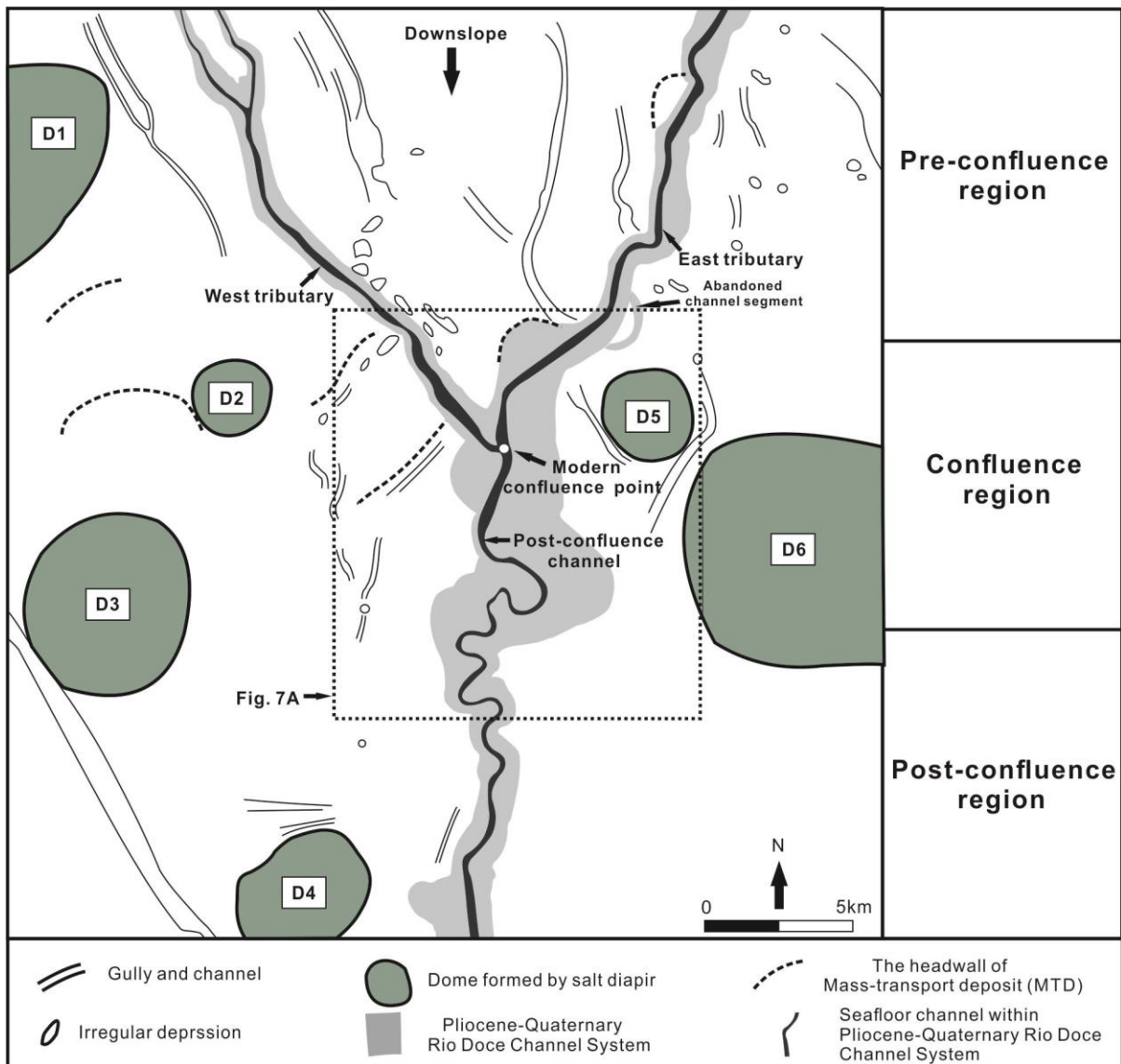


Figure 5

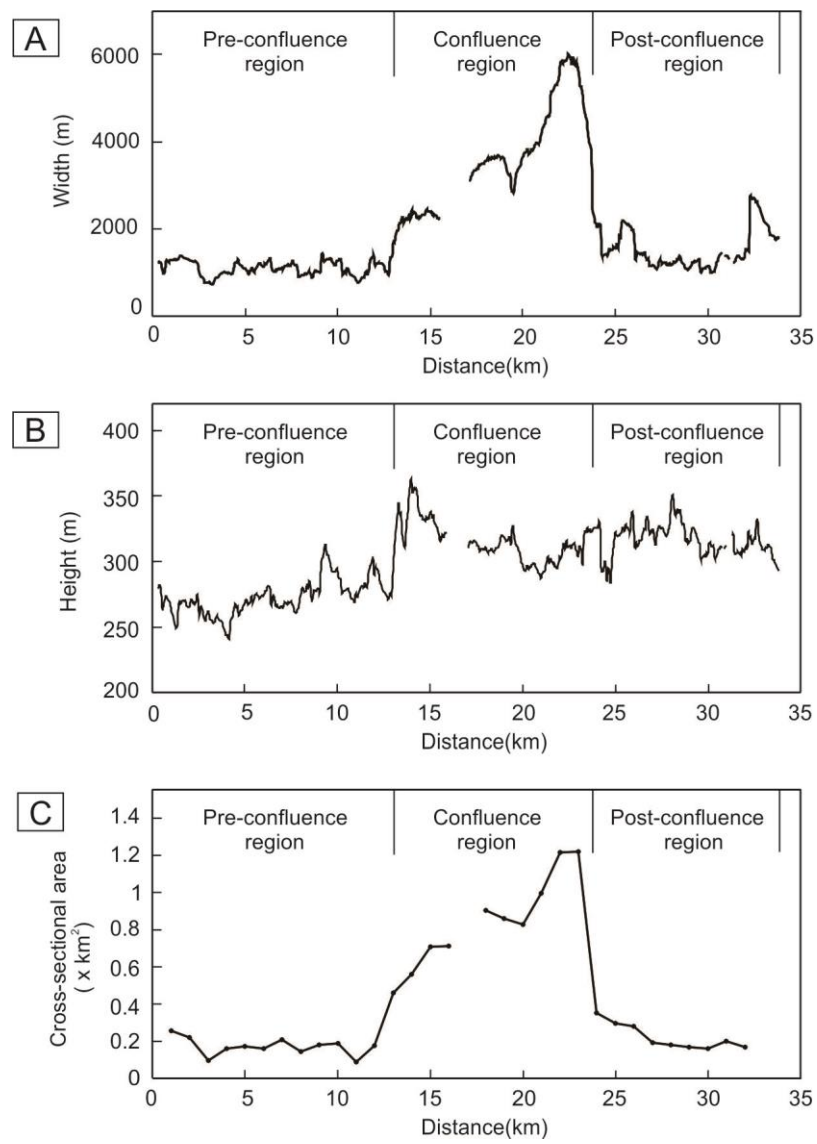


Figure 6

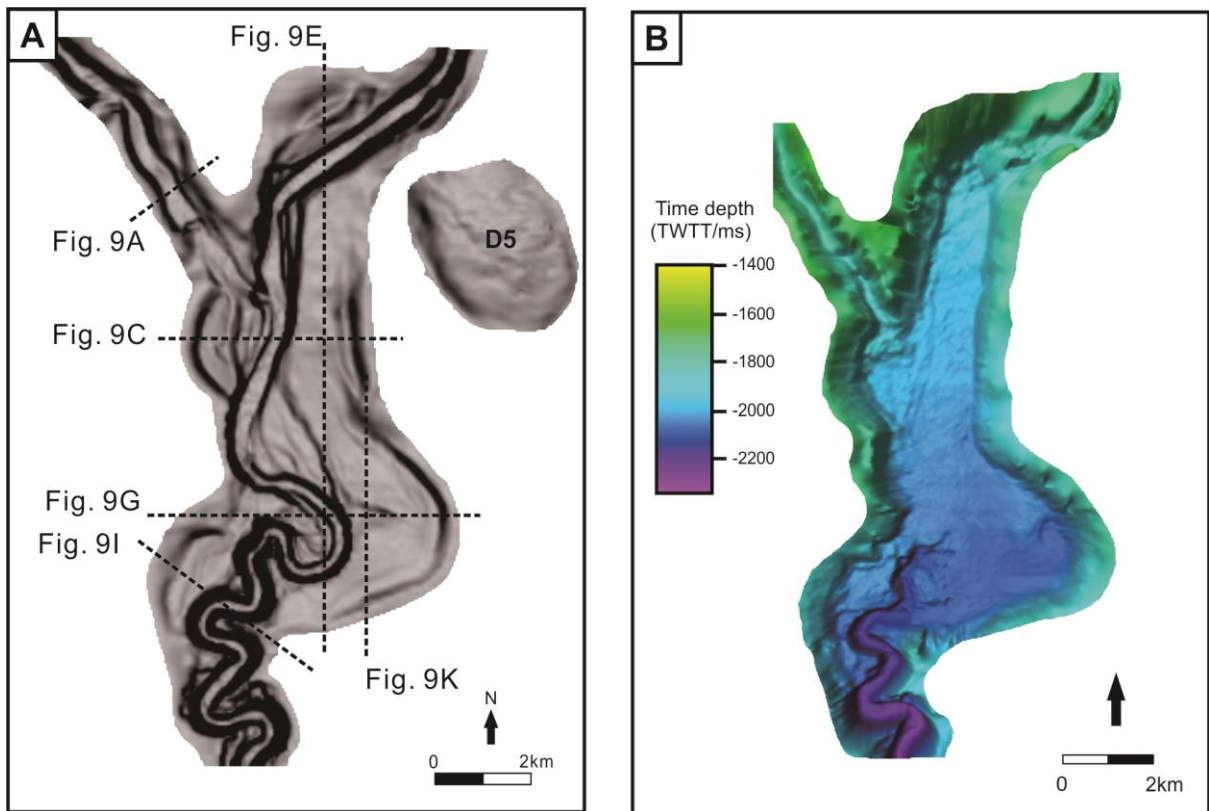


Figure 7

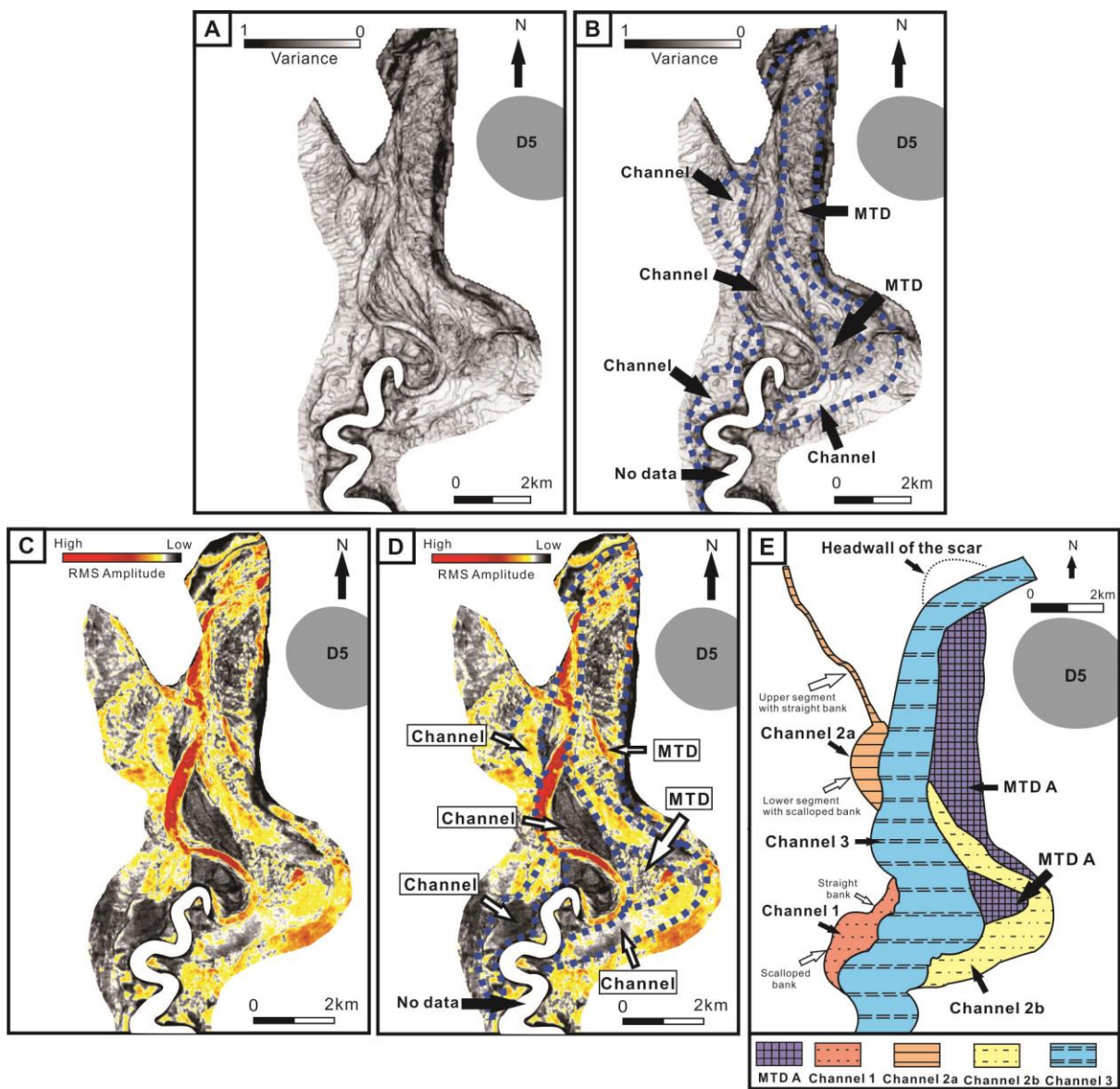


Figure 8

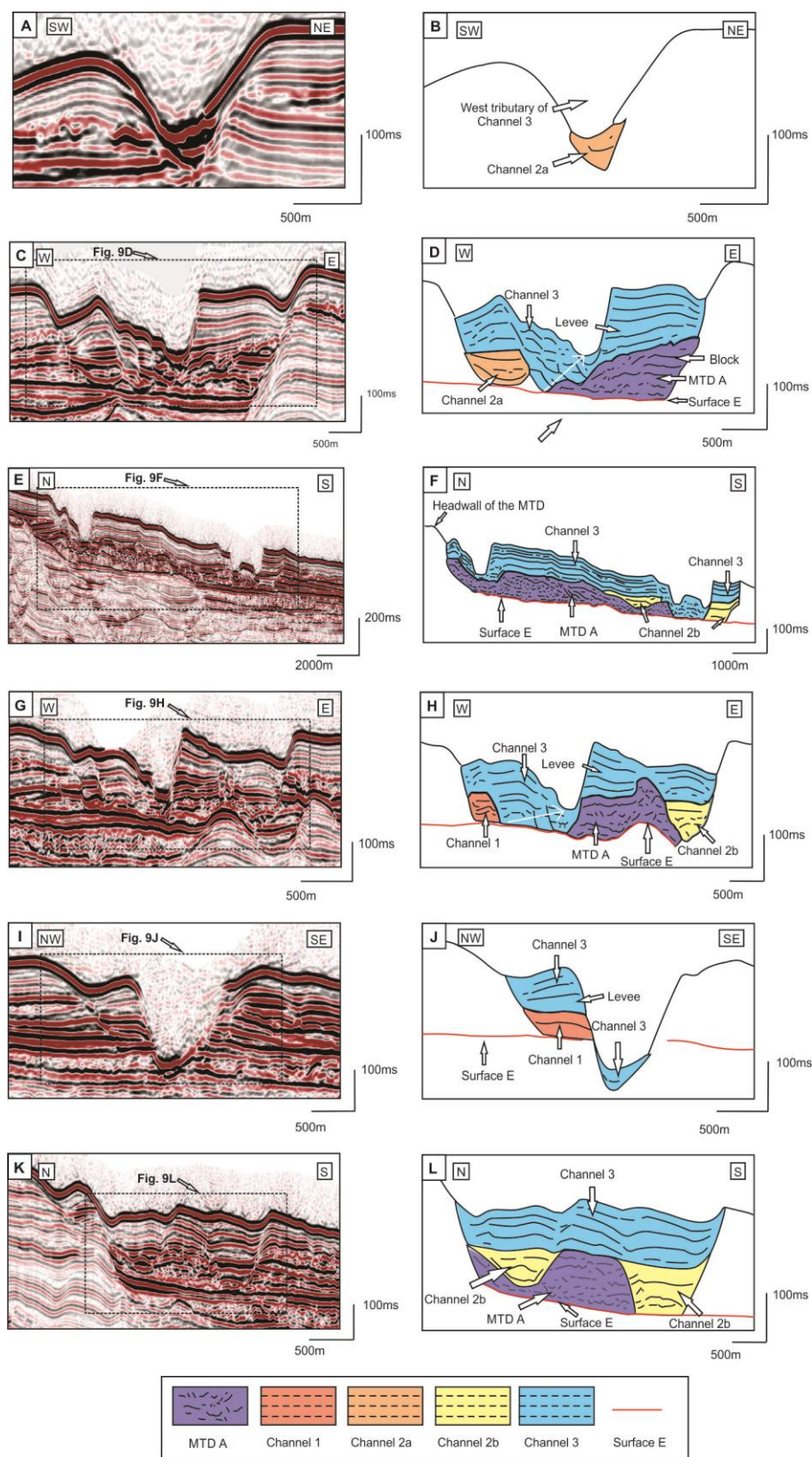


Figure 9

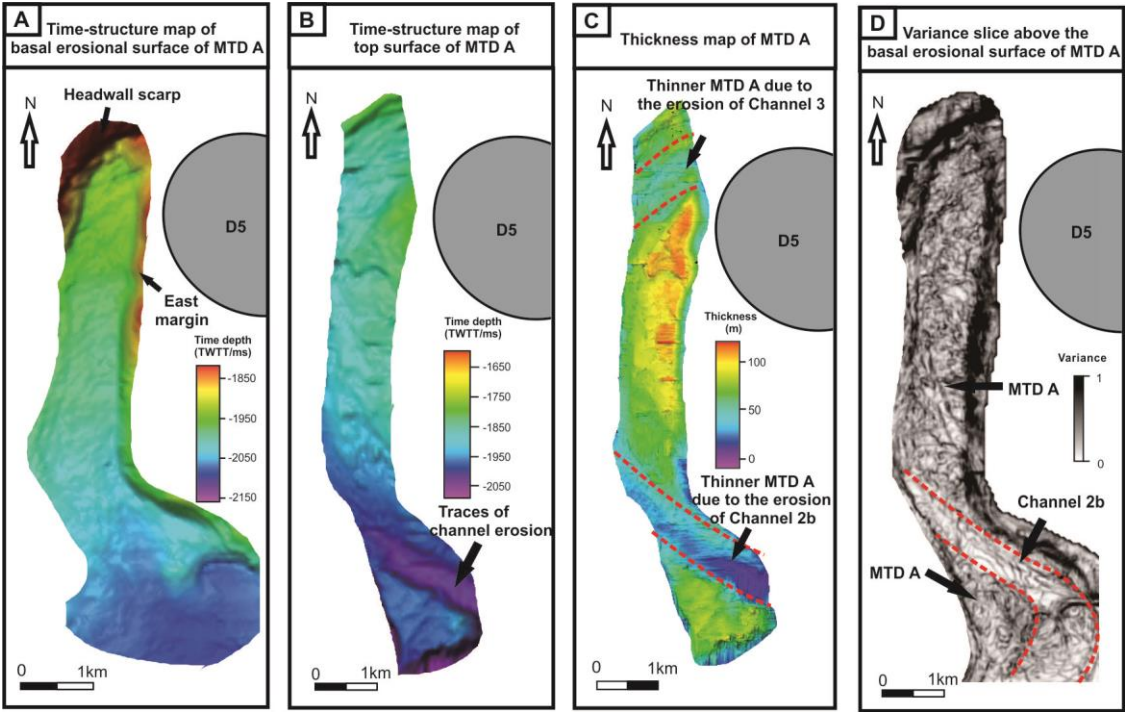


Figure 10

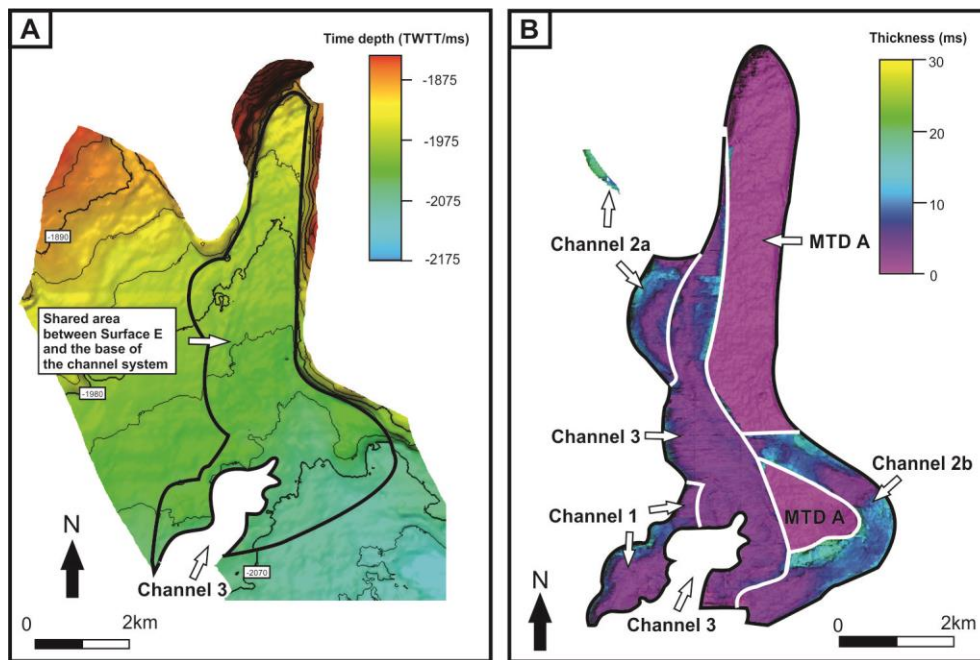


Figure 11

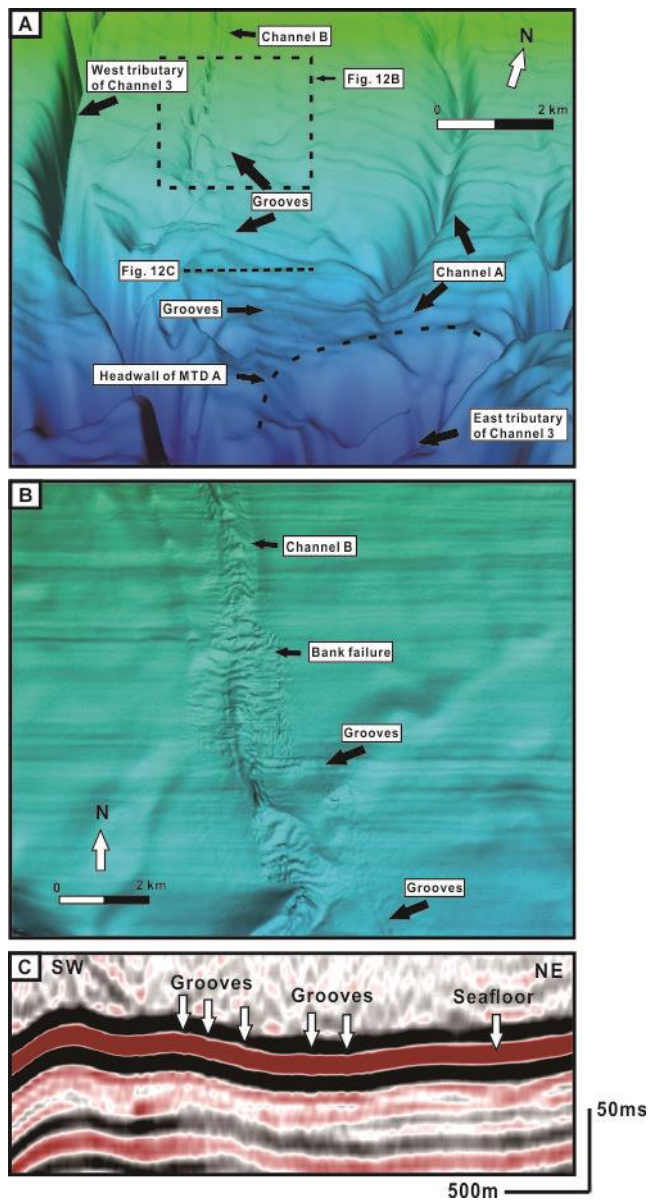


Figure 12

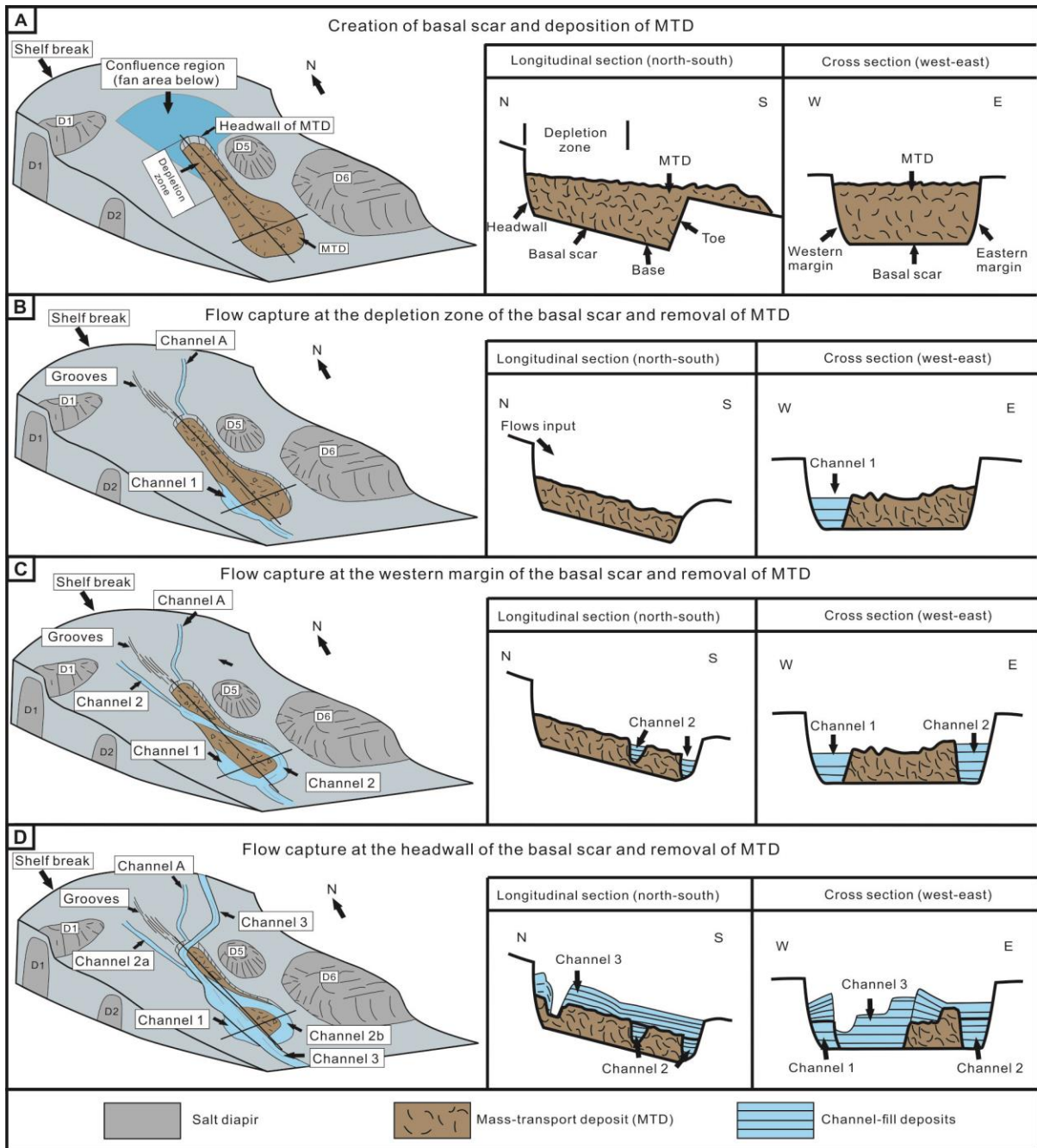


Figure 13